PLOS ONE

RESEARCH ARTICLE

Highly efficient UV/H_2O_2 technology for the removal of nifedipine antibiotics: Kinetics, co-existing anions and degradation pathways

Wenping Dong[1,2☯], Chuanxi Yang[3☯], Lingli Zhang[4], Qiang Su[1,2], Xiaofeng Zou[1,2], Wenfeng Xu[5], Xingang Gao[6], Kang Xie[7], Weiliang Wang[3]*

1 Shandong Academy of Environmental Science Co., Ltd., Jinan, China, **2** Shandong Huankeyuan Environmental Engineering Co., Ltd., Jinan, China, **3** School of Environmental and Municipal Engineering, Qingdao University of Technology, Qingdao, China, **4** Hi-tech Science Park Branch of Weihai Municipal Bureau of Ecological Environment, Weihai, China, **5** Shandong Think-eee Environmental Technology Co., Ltd., Jinan, China, **6** Qingdao Jiaming Measurement and Control Technology Co., Ltd., Qingdao, China, **7** School of Civil Engineering and Architecture, University of Jinan, Jinan, China

☯ These authors contributed equally to this work.
* sdqcsdnu@163.com

Check for updates

OPEN ACCESS

Citation: Dong W, Yang C, Zhang L, Su Q, Zou X, Xu W, et al. (2021) Highly efficient UV/H_2O_2 technology for the removal of nifedipine antibiotics: Kinetics, co-existing anions and degradation pathways. PLoS ONE 16(10): e0258483. https://doi.org/10.1371/journal.pone.0258483

Editor: Van-Huy Nguyen, Binh Duong University, VIET NAM

Received: June 24, 2021

Accepted: September 28, 2021

Published: October 28, 2021

Peer Review History: PLOS recognizes the benefits of transparency in the peer review process; therefore, we enable the publication of all of the content of peer review and author responses alongside final, published articles. The editorial history of this article is available here: https://doi.org/10.1371/journal.pone.0258483

Copyright: © 2021 Dong et al. This is an open access article distributed under the terms of the Creative Commons Attribution License, which permits unrestricted use, distribution, and reproduction in any medium, provided the original author and source are credited.

Data Availability Statement: All relevant data are within the manuscript and its Supporting Information files.

Abstract

This study investigates the degradation of nifedipine (NIF) by using a novel and highly efficient ultraviolet light combined with hydrogen peroxide (UV/H_2O_2). The degradation rate and degradation kinetics of NIF first increased and then remained constant as the H_2O_2 dose increased, and the quasi-percolation threshold was an H_2O_2 dose of 0.378 mmol/L. An increase in the initial pH and divalent anions (SO_4^{2-} and CO_3^{2-}) resulted in a linear decrease of NIF (the R^2 of the initial pH, SO_4^{2-} and CO_3^{2-} was 0.6884, 0.9939 and 0.8589, respectively). The effect of monovalent anions was complex; Cl^- and NO_3^- had opposite effects: low Cl^- or high NO_3^- promoted degradation, and high Cl^- or low NO_3^- inhibited the degradation of NIF. The degradation rate and kinetics constant of NIF *via* UV/H_2O_2 were 99.94% and 1.45569 min^{-1}, respectively, and the NIF concentration = 5 mg/L, pH = 7, the H_2O_2 dose = 0.52 mmol/L, T = 20 ˚C and the reaction time = 5 min. The ·OH was the primary key reactive oxygen species (ROS) and $\cdot O_2^-$ was the secondary key ROS. There were 11 intermediate products (P345, P329, P329-2, P315, P301, P274, P271, P241, P200, P181 and P158) and 2 degradation pathways (dehydrogenation of NIF → P345 → P274 and dehydration of NIF → P329 → P315).

1 Introduction

Water pollution is a major environmental problem the world is facing today, mainly due to modernization [1]. The removal of toxic organic pollutants discharged from the ever-increasing number of industries is a major environmental goal [2,3]. Nifedipine (NIF, Fig 1), 3,5-dimethyl 2,6-dimethyl-4-(2-nitrophenyl)-1,4-dihydropyridine-3,5-dicarboxylate, belongs to the dihydropyridine class of calcium channel antagonists and is one of the most useful pharmaceuticals for the treatment of hypertension, angina pectoris and other cardiovascular

Funding: This work was supported by the National Natural Science Foundation of China (41672340) and the Research and Demonstration of Special Reagents for Sewage Treatment Plant in Chemical Industry Park (RD28-2019).

Competing interests: The authors have declared that no competing interests exist.

disorders [4,5]. As a large portion of each administered dose is excreted from medical applications and the pharmaceutical industry, and a substantial amount of NIF is released to the environment [6]. It has been demonstrated that NIF residues in the environment can result in the evolution of novel antibiotic-resistant bacteria that ultimately pose a threat to the aquatic ecosystem and human health through human organ lesions and increased bacterial resistance [7,8]. Hence, the efficient removal of NIF from water is significant and essential to reducing environmental and ecological risks.

The removal of antibiotics from aqueous solutions has been widely researched, including removal by physical methods, chemical methods and biological methods [9–12]. Adsorption and advanced oxidation processes (AOPs, such as photocatalysis, Fenton, Fenton-like, photo-Fenton and catalytic ozonation) are the most promising wastewater treatment technologies for the removal of antibiotics from water environments and reduction of the resulting environmental risks because they are fast, efficient, low cost and convenient [13–16]. Many adsorbents have been employed for the eradication of antibiotics [17]. However, there are some drawbacks, such as incomplete removal, high energy requirements and the generation of toxic sludge and other waste products that entail further disposal [18]. Solar light-driven photocatalysis involves the photoinduced generation of holes (h^+) in the valence band (VB) and electrons (e^-) in the conduction band (CB) *via* light absorption by a semiconductor (TiO_2, ZnO and CdS). Sequential interfacial charge transfers release various reactive oxygen species (ROS), such as superoxide, peroxide, and hydroxyl radicals, which participate in the degradation of organic and inorganic pollutants [19–22]. However, the limitations of a wide bandgap, the rapid recombination rate of photogenerated electron-hole pairs, low solar light energy utilization efficiency, photocorrosion, and poor recyclability reduce the photocatalytic efficiency

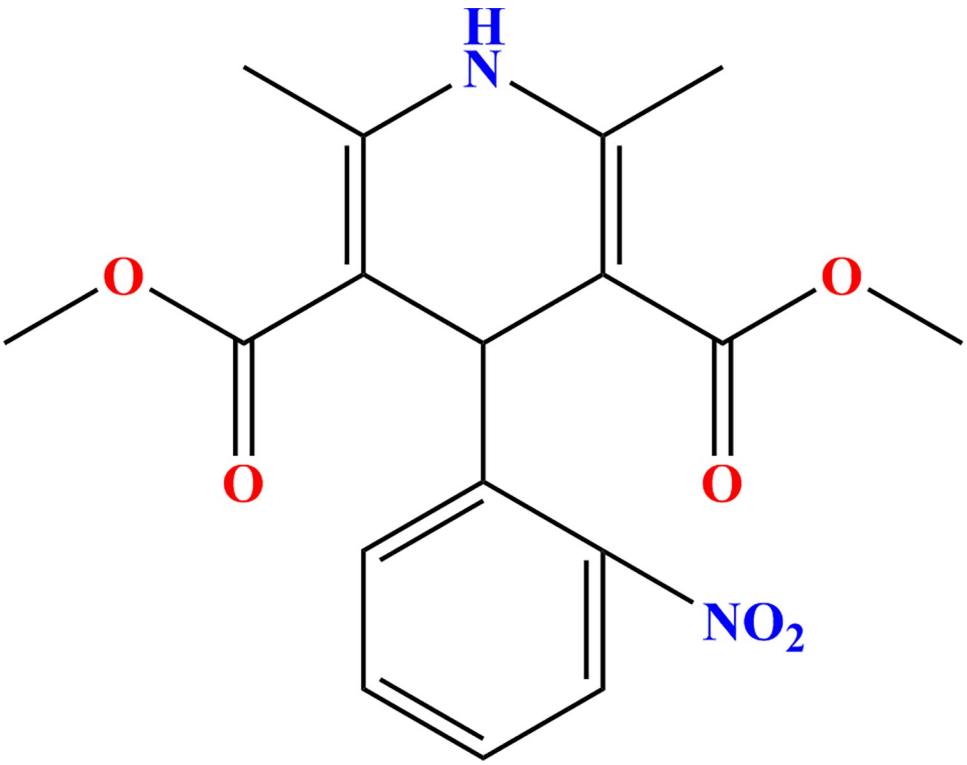

Fig 1. Structural formula of NIF.

https://doi.org/10.1371/journal.pone.0258483.g001

[23–25]. It is imperative to develop a novel Z-scheme system or heterojunction photocatalyst with broad photocatalytic applications [26,27]. However, limited research has focused on the removal of NIF from the water environment *via* AOPs. Therefore, it is important to study the removal of NIF *via* AOPs for the treatment of medical wastewater.

NIF is a known light-sensitive drug that degrades *via* intramolecular mechanisms to 4-(2-nitrophenyl) pyridine homolog (under UV light irradiation) and 4-(2-nitrosophenyl)-pyridine homolog (under daylight irradiation) [28]. Mojtaba Shamsipur et al. used a multivariate curve resolution method based on the combination of the Kubista approach and an iterative target transformation method by Gemperline to study the kinetics of NIF decomposition upon exposure to a 40 W lamp [29]. The results indicated that the photodecomposition kinetics of NIF are zero-order at the beginning of the reaction. However, when the reaction was more than 50% complete, the kinetics of the reaction changed to a first-order mechanism. The photo-degradation kinetics constants for the zero-order and first-order regions were (4.96 ±0.13)$^*10^{-9}$ M^{-1} s^{-1} and (6.22±0.10)$^*10^{-5}$ s^{-1}, respectively. This was the first study on the degradation of NIF, but the low degradation rate (65%) and kinetics limited the application of NIF removal *via* a photo-degradation system.

A novel method of UV light combined with hydrogen peroxide (UV/H_2O_2) is highly efficient, fast, and has a strong oxidizing ability; these advantages are attributed to the synergistic ability of UV light and H_2O_2 to generate ROS [30]. However, in UV/H_2O_2 AOPs, other constituents in water matrices may significantly affect the removal of target contaminants by competitively interacting with photons and ROS. In our previous study, the degradation of norfloxacin by using UV/H_2O_2 was investigated [31]. The degradation rate and apparent first-order kinetics constant of norfloxacin *via* UV/H_2O_2 were 98.8% and 0.22248 min^{-1}, respectively, and the norfloxacin concentration = 20 mg/L, the H_2O_2 dose = 1.2 mmol/L, the pH = 7, T = 20˚C and the reaction time = 20 min. The kinetics were low, and the formation mechanism of ROS was controversial, but it provided a novel research direction for the degradation of NIF *via* a UV/H_2O_2 system. Therefore, it should be noted that the degree of research to date on the degradation of NIF *via* UV/H_2O_2 oxidation processes is insufficient to thoroughly understand the fundamentals of ·OH generation, intermediate products and degradation pathways, which are important processes that must be considered in the design of wastewater treatment technology [32]. Furthermore, the effect of co-existing anions in the UV/H_2O_2 system may significantly affect the removal of NIF by competitively quenching with ROS [33]. Thus, it is still challenging to design a UV/H_2O_2 wastewater treatment technology with high efficiency.

On the one hand, the oxidizability of UV/H_2O_2 AOPs and removal rate of NIF were enhanced due to the combination between UV and H_2O_2 [30]. On the other hand, the anion (such as NO_3^-) was generated due to the degradation reaction between NIF and ROS. However, impacts of NO_3^- showed duality: it promotes the generation of ROS under irradiation, and also quenches the ROS of UV/H_2O_2 [32,33]. Hence, it is significant and meaningful to study the effect of co-existing anions on the degradation of NIF via UV/H_2O_2 AOPs. To better understand the removal efficacy of a target compound by UV/H_2O_2 AOPs in different real water environments, the divalent anions (SO_4^{2-} and CO_3^{2-}) and monovalent anions (Cl^- and NO_3^-) have been developed to model the impact of water constituents on the reaction kinetics.

The aims of this study were to demonstrate the application of NIF degradation and to evaluate the performance and mechanism of UV/H_2O_2 AOPs. The specific objectives were (1) to assess the effect of the H_2O_2 dose, initial pH, and co-existing anions (SO_4^{2-}, CO_3^{2-}, Cl^- and NO_3^-) on the degradation of UV/H_2O_2, (2) to predict the key ROS of the UV/H_2O_2 method and (3) to propose the degradation pathway of NIF.

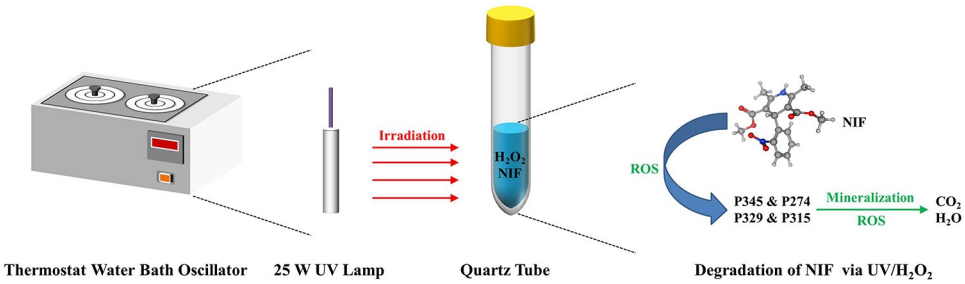

Fig 2. Experimental setup of UV/H_2O_2.

https://doi.org/10.1371/journal.pone.0258483.g002

2 Materials and methods

2.1 Chemicals

NIF was purchased from Shanghai Aladdin Bio-Chem Technology Co., Ltd. (Shanghai, China). Hydrogen peroxide (H_2O_2), hydrochloric acid (HCl), sodium hydroxide (NaOH), sodium sulfate (Na_2SO_4), sodium carbonate (Na_2CO_3), sodium nitrate ($NaNO_3$) and sodium chloride (NaCl) were purchased from Sinopharm Chemical Reagent Co., Ltd. (Shanghai, China). Methyl alcohol (CH_3OH) was purchased from Thermo Fisher Scientific (Shanghai, China). All chemicals and reagents used were of analytical grade or higher and directly used without further purification. All solutions were prepared with deionized water.

2.2 Experimental setup

The UV/H_2O_2 degradation experiments (Fig 2) were conducted in deionized water with the addition of H_2O_2 to the sample prior to 25 W UV light source exposure (254 nm). The initial NIF concentration was 5 mg/L, the temperature was 20˚C, the H_2O_2 dose was 0–1.04 mmol/L and the pH was 4–10. To understand the effect of co-existing anions, different sources of SO_4^{2-}, CO_3^{2-}, Cl^- and NO_3^- (from 5 to 50 mg/L) were added to the NIF degradation experiments to evaluate the removal rate and degradation kinetics.

2.3 Removal rate and degradation kinetics

The removal rate (η) of NIF under UV/H_2O_2 was calculated using Eq 1 (Eq 1):

$$\eta = \frac{C_0 - C_t}{C_0} \times 100\% \quad \text{(Eq 1)}$$

where C_0 is the initial concentration of NIF and C_t is the concentration of NIF at a certain degradation time, which was determined from the liquid chromatogram (S1 and S2 Figs).

The degradation kinetics of NIF *via* UV/H_2O_2 followed the apparent first-order kinetic law, and the apparent first-order kinetic constant (k'_{app}) was described by Eq 2 (Eq 2):

$$-\ln\frac{C_t}{C_0} = k'_{app}t \quad \text{(Eq 2)}$$

where t is the reaction time.

2.4 Organics analysis

NIF and its intermediate products in the UV/H_2O_2 degradation reaction solutions were analyzed by an Agilent 1260 series liquid chromatogram mass spectrometry (LC-Q-TOF-MS)

system (Agilent, USA) with a C18 column (100 mm × 2.1 mm, 3.5 mm). The wavelength was 237 nm according to ultraviolet and visible spectrophotometry (S1 Fig). The mobile phase was methyl alcohol and deionized water at 63:35 (v/v). The drying gas of N_2 was 8.0 mL/min, and the testing time was 30 min.

2.5 Electron spin resonance (ESR) measurements

ESR measurements were performed with a JES-FA200 electron spin resonance spectrometer and used to measure the hydroxide radical (·OH) and superoxide radical ($\cdot O_2^-$) during the degradation of NIF under UV/H_2O_2 using 5,5-dimethyl-1-pyrroline N-oxide (DMPO) as the spin trapping reagent.

3 Results and discussion

3.1 Effect of H_2O_2 dose

In general, the H_2O_2 dose significantly affects the oxidative degradation of antibiotics by controlling the generation rate of ROS, and the effect of H_2O_2 dose has been shown to have a dual nature. The specific degradation performance of NIF was enhanced by increasing the dose of H_2O_2 when it was low; however, the degradation performance of NIF increased slowly, remained constant or decreased when the H_2O_2 dose was high. As shown in Fig 3A and 3B and S1 Table, the degradation rates of NIF under UV/H_2O_2 were 72.81% (0 mmol/L) < 95.97% (0.13 mmol/L) < 99.31% (0.26 mmol/L) < 99.94% (0.52 mmol/L) < 99.95% (1.04 mmol/L), the kinetics constants k'_{app} were 0.2560 min^{-1} (0 mmol/L) < 0.6752 min^{-1} (0.13 mmol/L) < 1.03947 min^{-1} (0.26 mmol/L) < 1.45569 min^{-1} (0.52 mmol/L) < 1.59404 min^{-1} (1.04 mmol/L), and the $t_{1/2}$ (time of NIF degradation rate = 50%) were 0.4 min (0.52 mmol/L) < 0.6 min (1.04 mmol/L) < 1.0 min (0.26 mmol/L) < 1.5 min (0.13 mmol/L) < 2.8 min (0 mmol/L) when the NIF concentration = 5 mg/L, the H_2O_2 dose = 0–1.04 mmol/L, the pH = 7, T = 20 ˚C and the reaction time = 5 min. As shown in Fig 3C, the effect of the H_2O_2 dose on the degradation of NIF *via* UV/H_2O_2 system had a dual nature. The degradation kinetics constant noticeably increased as the H_2O_2 dose increased and then remained constant at 1.5±0.1 min^{-1}. When the H_2O_2 dose was < 0.52 mmol/L, the slope was 3.013 (min^{-1})/(mmol/L), but it decreased to 0.266 (min^{-1})/(mmol/L) when the H_2O_2 dose was > 0.52 mmol/L; hence, the quasi-percolation threshold (QPT) of the H_2O_2 dose was 0.378 mmol/L [34]. This trend was based on the generation and quenching of ·OH described by (Eq 3) to (Eq 6) [35]:

$$\text{(a) } H_2O_2 \text{ dose} < \text{QPT}:$$

$$H_2O_2 \rightarrow 2 \cdot OH \quad \text{(Eq 3)}$$

$$\text{(b) } H_2O_2 \text{ dose} > \text{QPT}:$$

$$H_2O_2 + \cdot OH \rightarrow \cdot HO_2 + H_2O \quad \text{(Eq 4)}$$

$$\cdot HO_2 + \cdot OH \rightarrow H_2O + O_2 \quad \text{(Eq 5)}$$

$$2 \cdot OH \rightarrow H_2O_2 \quad \text{(Eq 6)}$$

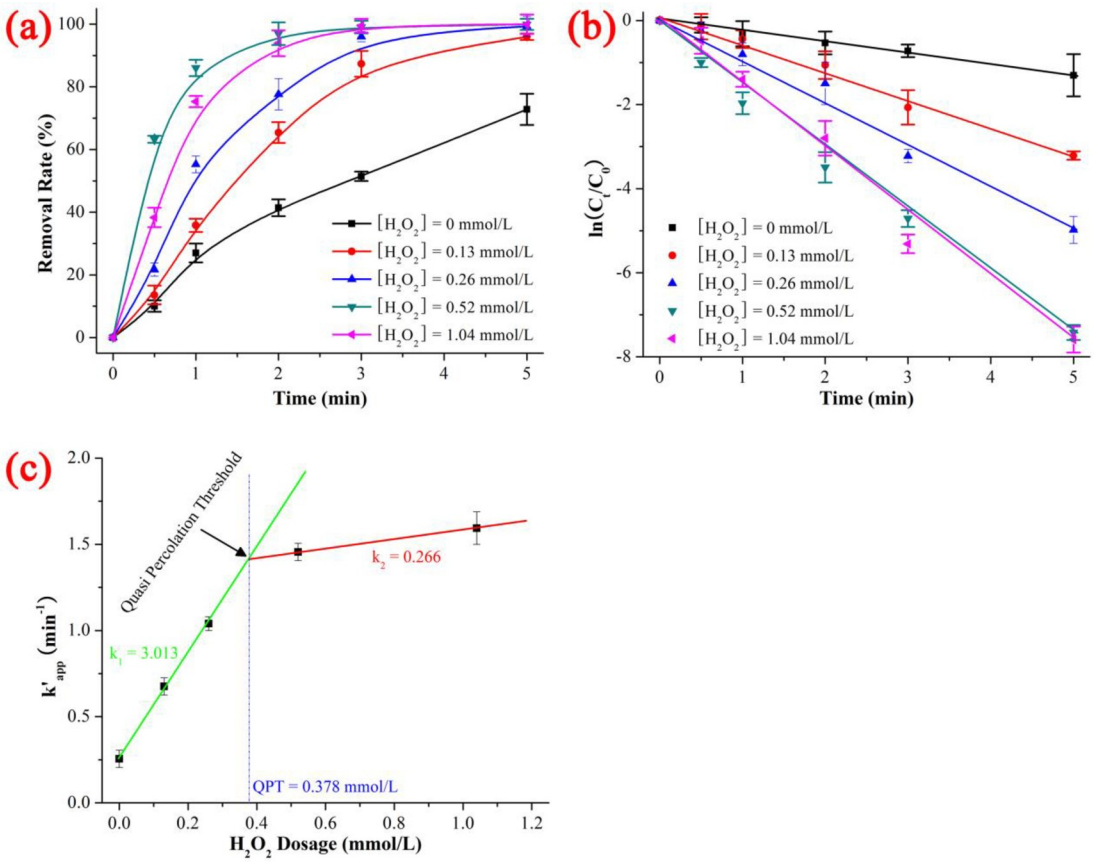

Fig 3. Effect of H_2O_2 dose on removal rate (a), kinetics constant (b) and linear fitting between kinetics constant and H_2O_2 dose on the degradation of NIF *via* UV/H_2O_2. The error bars represent the standard deviation (n = 3).

https://doi.org/10.1371/journal.pone.0258483.g003

3.2 Effect of initial pH

The pH is another key parameter of the UV/H_2O_2 system. It significantly affects the oxidative degradation of antibiotics by transforming the protonation states and changing the redox potential at different pH values. As shown in Fig 4A and 4B and S2 Table, the degradation rates of NIF under UV/H_2O_2 was 97.54% (pH = 10) < 98.69% (pH = 8) < 99.77% (pH = 5) < 99.94% (pH = 4 and 7), the kinetics constant k'_{app} was 0.75217 min^{-1} (pH = 10) < 0.91269 min^{-1} (pH = 8) < 1.21831 min^{-1} (pH = 5) < 1.45569 min^{-1} (pH = 7) < 1.51175 min^{-1} (pH = 4), and the $t_{1/2}$ was 0.4 min (pH = 7) < 0.7 min (pH = 4) < 0.8 min (pH = 5) < 0.9 min (pH = 8) < 1.1 min (pH = 10) when the NIF concentration = 5 mg/L, pH = 4–10, H_2O_2 dose = 0.52 mmol/L, T = 20 ˚C and reaction time = 5 min. As shown in Fig 4C, the degradation kinetics of NIF *via* UV/H_2O_2 system exhibited a poor linear decrease as the pH increased (y = -0.1155x + 1.95533, R^2 = 0.6884). The results indicated that acidic solution (pH = 4) was more favorable for degrading NIF than basic solution (pH = 10) under UV/H_2O_2. The possible reasons were in accord with the redox potential, generation rate of ROS and reaction rate between ROS and NIF. The inhibiting effect of the basic solution was due to the quenching reaction between OH^- and ·OH, which is shown in (Eq 7) to (Eq 11) [36]:

$$H_2O_2 \rightarrow HO_2^- + H^+ \quad \text{(Eq 7)}$$

$$H^+ + OH^- \rightarrow H_2O \quad \text{(Eq 8)}$$

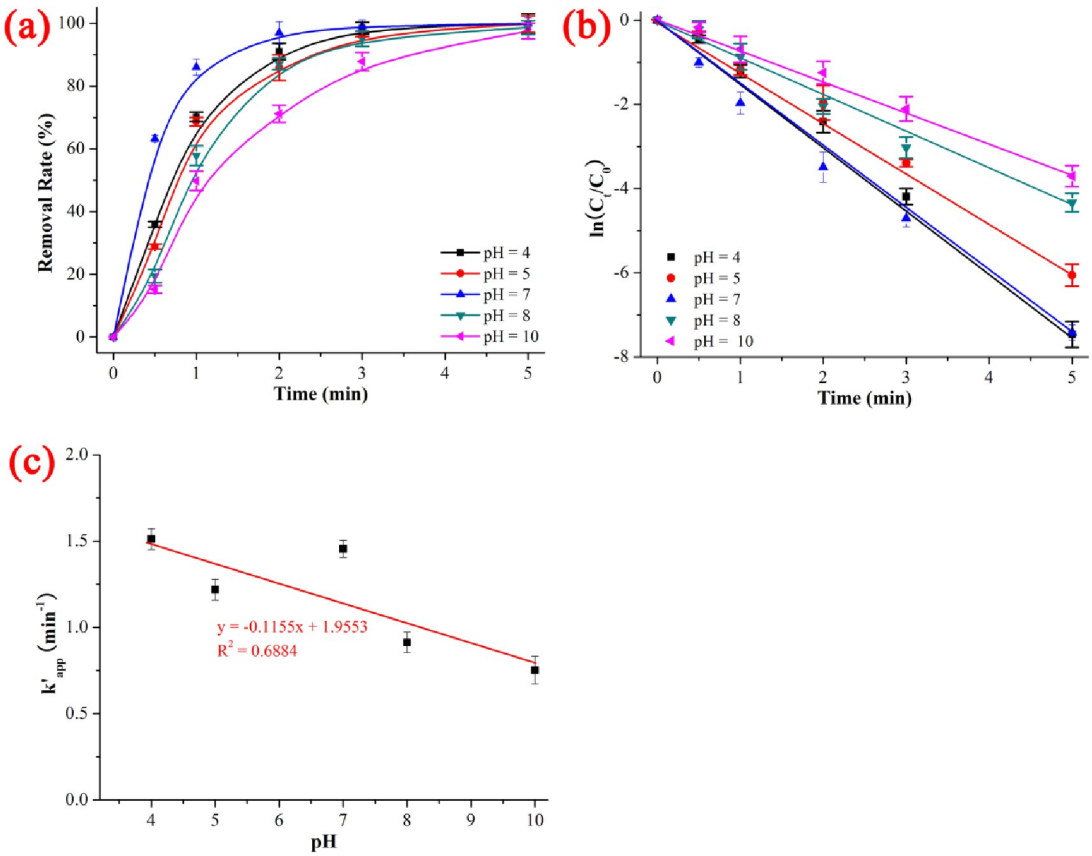

Fig 4. Effect of initial pH on the removal rate (a), kinetics constant (b) and linear fitting between kinetics constant and initial pH on the degradation of NIF *via* UV/H_2O_2. The error bars represent the standard deviation (n = 3).

https://doi.org/10.1371/journal.pone.0258483.g004

$$H_2O_2 + HO_2^- \rightarrow H_2O + OH^- + O_2 \quad \text{(Eq 9)}$$

$$\cdot OH + HO_2^- \rightarrow OH^- + \cdot HO_2 \quad \text{(Eq 10)}$$

$$\cdot OH + HO_2^- \rightarrow H_2O + \cdot O_2^- \quad \text{(Eq 11)}$$

3.3 Effect of SO_4^{2-}

It is important to evaluate the effect of co-existing anions (such as SO_4^{2-}, CO_3^{2-}, Cl^- and NO_3^-) because the co-existing anions in wastewater impact the degradation capacity and the oxidation mechanism of ROS.

As shown in Fig 5A and 5B and S3 Table, the degradation rates of NIF under UV/H_2O_2 with different SO_4^{2-} concentrations were 99.26% (SO_4^{2-} concentration = 50 mg/L) < 99.81% (SO_4^{2-} concentration = 20 mg/L) < 99.93% (SO_4^{2-} concentration = 5 mg/L) < 99.94% (SO_4^{2-} concentration = 0 mg/L), the kinetics constant k'_{app} was 1.00154 min^{-1} (SO_4^{2-} concentration = 50 mg/L) < 1.24540 min^{-1} (SO_4^{2-} concentration = 20 mg/L) < 1.38175 min^{-1} (SO_4^{2-} concentration = 5 mg/L) < 1.45569 min^{-1} (SO_4^{2-} concentration = 0 mg/L), and the $t_{1/2}$ was 0.4 min (SO_4^{2-} concentration = 0 mg/L and 5 mg/L) < 0.6 min (SO_4^{2-} concentration = 20 mg/L) < 0.8 min (SO_4^{2-} concentration = 50 mg/L) when the NIF concentration = 5 mg/L, SO_4^{2-}

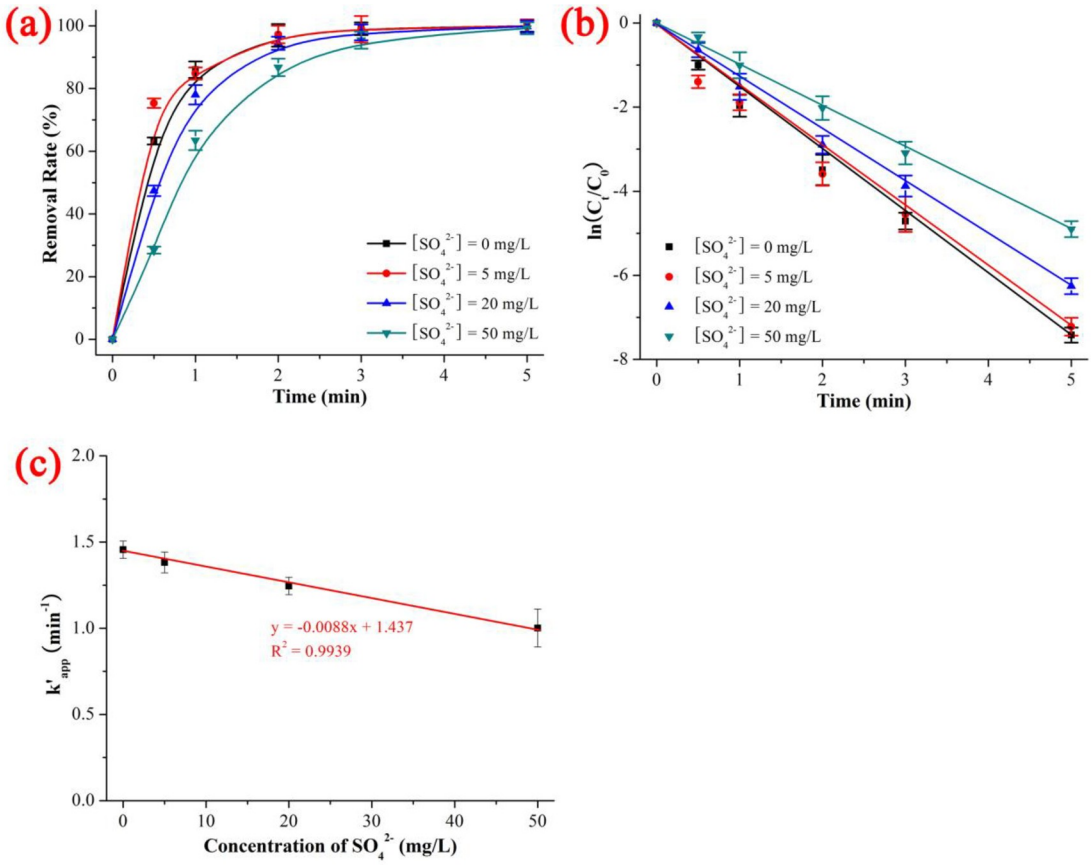

Fig 5. Effect of SO_4^{2-} on the removal rate (a), kinetics constant (b) and linear fitting between kinetics constant and concentration of SO_4^{2-} on the degradation of NIF *via* UV/H_2O_2. The error bars represent the standard deviation (n = 3).

https://doi.org/10.1371/journal.pone.0258483.g005

concentration = 0–50 mg/L, pH = 7, H_2O_2 dose = 0.52 mmol/L, T = 20 ˚C and reaction time = 5 min. As shown in Fig 5C, the degradation kinetics of NIF *via* UV/H_2O_2 system exhibited a good linear decrease as the SO_4^{2-} concentration increased (y = -0/0088x + 1.437, R^2 = 0.9939). The inhibition effect was 5.08% (SO_4^{2-} concentration = 5 mg/L) < 14.45% (SO_4^{2-} concentration = 20 mg/L) < 31.20% (SO_4^{2-} concentration = 50 mg/L), which was in keeping with the trend of the kinetics constants: 1.00154 min^{-1} (SO_4^{2-} concentration = 50 mg/L) < 1.24540 min^{-1} (SO_4^{2-} concentration = 20 mg/L) < 1.38175 min^{-1} (SO_4^{2-} concentration = 5 mg/L). The degradation rate of NIF decreased with increasing SO_4^{2-} concentration, and the quenching mechanism of ROS *via* SO_4^{2-} is shown in (Eq 12) to (Eq 17) [37]:

$$H^+ + SO_4^{2-} \rightarrow HSO_4^- \quad \text{(Eq 12)}$$

$$HSO_4^- + \cdot OH \rightarrow SO_4\cdot^- + H_2O \quad \text{(Eq 13)}$$

$$SO_4\cdot^- + H_2O \rightarrow H^+ + SO_4^{2-} + \cdot OH \quad \text{(Eq 14)}$$

$$SO_4\cdot^- + H_2O_2 \rightarrow H^+ + SO_4^{2-} + H_2O \quad \text{(Eq 15)}$$

$$SO_4\cdot^- + H_2O\cdot \rightarrow H^+ + SO_4^{2-} + O_2 \quad \text{(Eq 16)}$$

$$SO_4\cdot^- + e^- \rightarrow SO_4^{2-} \quad \text{(Eq 17)}$$

3.4 Effect of CO_3^{2-}

As shown in Fig 6A and 6B and S4 Table, the degradation rates of NIF under UV/H_2O_2 with different CO_3^{2-} concentrations was 99.41% (CO_3^{2-} concentration = 50 mg/L) < 99.71% (CO_3^{2-} concentration = 20 mg/L) < 99.85% (CO_3^{2-} concentration = 5 mg/L) < 99.94% (CO_3^{2-} concentration = 0 mg/L), the kinetics constant k'_{app} was 1.04447 min^{-1} (CO_3^{2-} concentration = 50 mg/L) < 1.16907 min^{-1} (CO_3^{2-} concentration = 20 mg/L) < 1.29550 min^{-1} (CO_3^{2-} concentration = 5 mg/L) < 1.45569 min^{-1} (CO_3^{2-} concentration = 0 mg/L), and the $t_{1/2}$ was 0.4 min (CO_3^{2-} concentration = 0 mg/L) < 0.5 min (CO_3^{2-} concentration = 5 mg/L) < 0.6 min (CO_3^{2-} concentration = 20 mg/L) < 0.7 min (CO_3^{2-} concentration = 50 mg/L) when the NIF concentration = 5 mg/L, CO_3^{2-} concentration = 0–50 mg/L, pH = 7, H_2O_2 dose = 0.52 mmol/L, T = 20 ˚C and reaction time = 5 min. As shown in Fig 6C, the degradation kinetics of NIF *via* the UV/H_2O_2 system exhibited a good linear decrease as the CO_3^{2-} concentration increased (y = -0.0072x + 1.3771, R^2 = 0.8589). The inhibition trend was 11.00% (CO_3^{2-} concentration = 5 mg/L) < 19.69% (CO_3^{2-} concentration = 20 mg/L) < 28.25% (CO_3^{2-} concentration = 50 mg/L), which was in keeping with that of kinetics constant: 1.04447 min^{-1} (CO_3^{2-} concentration = 50 mg/L) < 1.16907 min^{-1} (CO_3^{2-} concentration = 20 mg/L) < 1.29550 min^{-1} (CO_3^{2-} concentration = 5 mg/L). The degradation rate of NIF decreased with increasing CO_3^{2-} concentration, and the quenching mechanism of the ROS *via* CO_3^{2-} is shown in (Eq 18) to (Eq 22) [38]:

$$CO_3^{2-} + H^+ \rightarrow HCO_3^- \quad \text{(Eq 18)}$$

$$HCO_3^- \rightarrow CO_3^{2-} + H^+ \quad \text{(Eq 19)}$$

$$CO_3^{2-} + \cdot OH \rightarrow CO_3^{\cdot -} + OH^- \quad \text{(Eq 20)}$$

$$HCO_3^- + \cdot OH \rightarrow CO_3^{\cdot -} + H_2O \quad \text{(Eq 21)}$$

$$CO_3^{\cdot -} + H_2O_2 \rightarrow HO_2\cdot + HCO_3^- \quad \text{(Eq 22)}$$

3.5 Effect of Cl^-

As shown in Fig 7A and 7B and S5 Table, the degradation rates of NIF under UV/H_2O_2 with different Cl^- concentrations was 99.57% (Cl^- concentration = 50 mg/L) < 99.94% (Cl^- concentration = 0 mg/L) < 99.98% (Cl^- concentration = 20 mg/L) < 100% (Cl^- concentration = 5 mg/L), the kinetics constant k'_{app} was 1.09588 min^{-1} (Cl^- concentration = 50 mg/L) < 1.45569 min^{-1} (Cl^- concentration = 0 mg/L) < 1.72666 min^{-1} (Cl^- concentration = 20 mg/L) < 1.98350 min^{-1} (Cl^- concentration = 5 mg/L), and the $t_{1/2}$ was 0.3 min (Cl^- concentration = 5 mg/L and 20 mg/L) < 0.4 min (Cl^- concentration = 0 mg/L) < 0.9 min (Cl^- concentration = 50 mg/L) when the NIF concentration = 5 mg/L, Cl^- concentration = 0–50 mg/L, pH = 7, H_2O_2 dosage = 0.52 mmol/L, T = 20 ˚C and reaction time = 5 min. As shown in Fig 7C, although the degradation kinetics of NIF *via* UV/H_2O_2 system decreased with increasing Cl^- concentration, the effect of Cl^- on the degradation of NIF had a dual nature: low Cl^- concentrations promoted the degradation of NIF, while high Cl^- concentrations inhibited the degradation of NIF. The degradation kinetics of NIF *via* UV/H_2O_2 system exhibited a poor linear decrease as the Cl^- concentration increased (y = -0.012x + 1.7897, R^2 = 0.5013). The trend of inhibition was

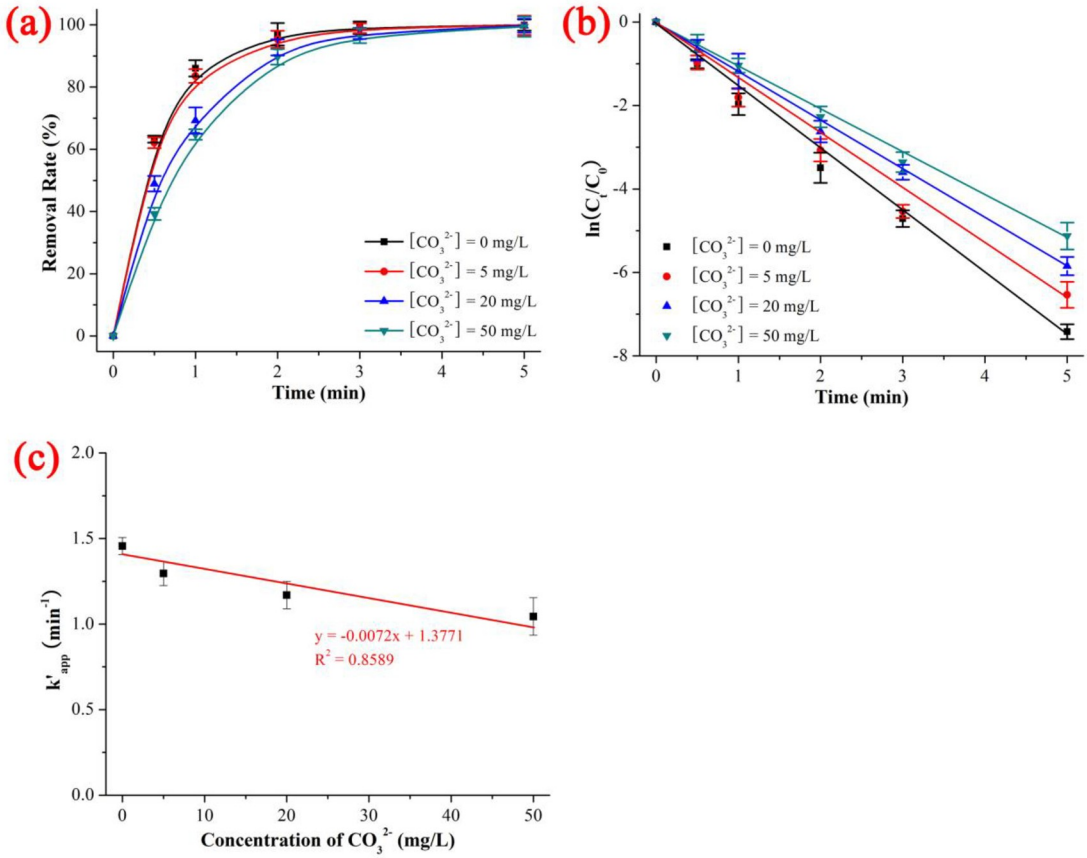

Fig 6. Effect of CO_3^{2-} on the removal rate (a), kinetics constant (b) and linear fitting between kinetics constant and concentration of CO_3^{2-} on the degradation of NIF *via* UV/H_2O_2. The error bars represent the standard deviation (n = 3).

https://doi.org/10.1371/journal.pone.0258483.g006

-36.25% (Cl^- concentration = 5 mg/L) < -18.61% (Cl^- concentration = 20 mg/L) < 24.71% (Cl^- concentration = 50 mg/L), which was in keeping with the trend of kinetics constant: 1.09588 min^{-1} (Cl^- concentration = 50 mg/L) < 1.72666 min^{-1} (Cl^- concentration = 20 mg/L) < 1.98350 min^{-1} (Cl^- concentration = 5 mg/L). The reaction mechanism between Cl^- and ·OH is shown in (Eq 23) to (Eq 27) [39]:

$$Cl^- + \cdot OH \rightarrow Cl\cdot + OH^- \quad \text{(Eq 23)}$$

$$Cl\cdot + Cl^- \rightarrow \cdot Cl_2^- \quad \text{(Eq 24)}$$

$$\cdot Cl_2^- + H_2O_2 \rightarrow H^+ + 2Cl^- + H_2O\cdot \quad \text{(Eq 25)}$$

$$\cdot OH + Cl^- \rightarrow \cdot HOCl^- \quad \text{(Eq 26)}$$

$$\cdot HOCl^- + H^+ \rightarrow H_2O + Cl^- \quad \text{(Eq 27)}$$

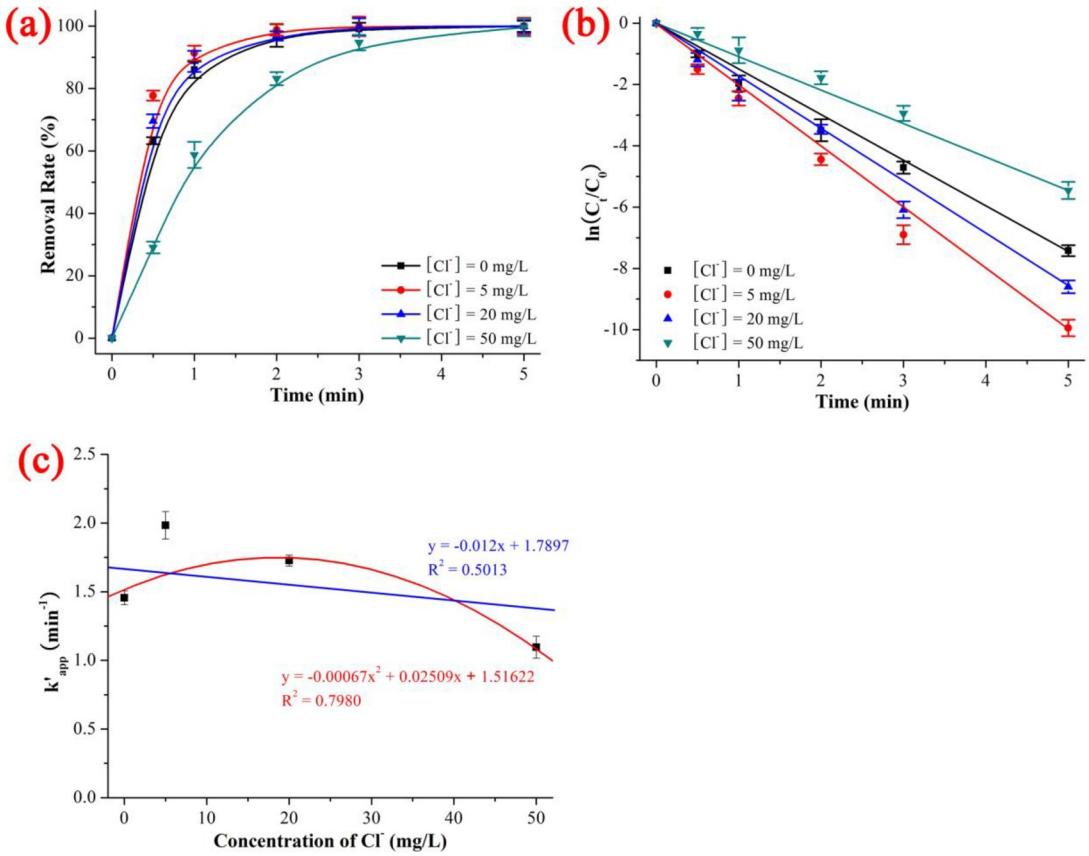

Fig 7. Effect of CO_3^{2-} on the removal rate (a), kinetics constant (b) and linear fitting between kinetics constant and concentration of CO_3^{2-} on the degradation of NIF *via* UV/H_2O_2. The error bars represent the standard deviation (n = 3).

https://doi.org/10.1371/journal.pone.0258483.g007

3.6 Effect of NO_3^-

As shown in Fig 8A and 8B and S6 Table, the degradation rates of NIF under UV/H_2O_2 with different NO_3^- concentrations was 99.45% (NO_3^- concentration = 5 mg/L) < 99.89% (NO_3^- concentration = 20 mg/L) < 99.94% (NO_3^- concentration = 0 mg/L) < 99.97% (NO_3^- concentration = 50 mg/L), the kinetics constant k'_{app} was 1.03215 min^{-1} (NO_3^- concentration = 5 mg/L) < 1.29801 min^{-1} (NO_3^- concentration = 20 mg/L) < 1.45569 min^{-1} (NO_3^- concentration = 0 mg/L) < 1.55295 min^{-1} (NO_3^- concentration = 50 mg/L), and the $t_{1/2}$ was 0.3 min (NO_3^- concentration 50 mg/L) < 0.4 min (NO_3^- concentration = 0 mg/L and 20 mg/L) < 0.6 min (NO_3^- concentration = 5 mg/L) when the NIF concentration = 5 mg/L, NO_3^- concentration = 0–50 mg/L, pH = 7, H_2O_2 dose = 0.52 mmol/L, T = 20˚C and reaction time = 5 min. As shown in Fig 8C, NO_3^- had the opposite effect on the degradation of NIF *via* the UV/H_2O_2 system compared to Cl^-. The effect of NO_3^- on the degradation of NIF had a dual nature: low NO_3^- concentrations inhibited the degradation of NIF, but high NO_3^- concentrations promoted the degradation of NIF. The degradation kinetics of NIF *via* the UV/H_2O_2 system showed a poor linear decrease with increasing NO_3^- concentration (y = -0.005377x + 1.31881, R^2 = 0.4514). The inhibition effect was -6.68% (NO_3^- concentration = 50 mg/L) < 10.83% (NO_3^- concentration = 20 mg/L) < 29.10% (NO_3^- concentration = 5 mg/L), which was in keeping with the trend of the kinetics constant: 1.03215 min^{-1} (NO_3^- concentration = 5 mg/L) < 1.29801 min^{-1} (NO_3^- concentration = 20 mg/L) < 1.55295 min^{-1} (NO_3^- concentration = 50 mg/L). The mechanism of the reaction between

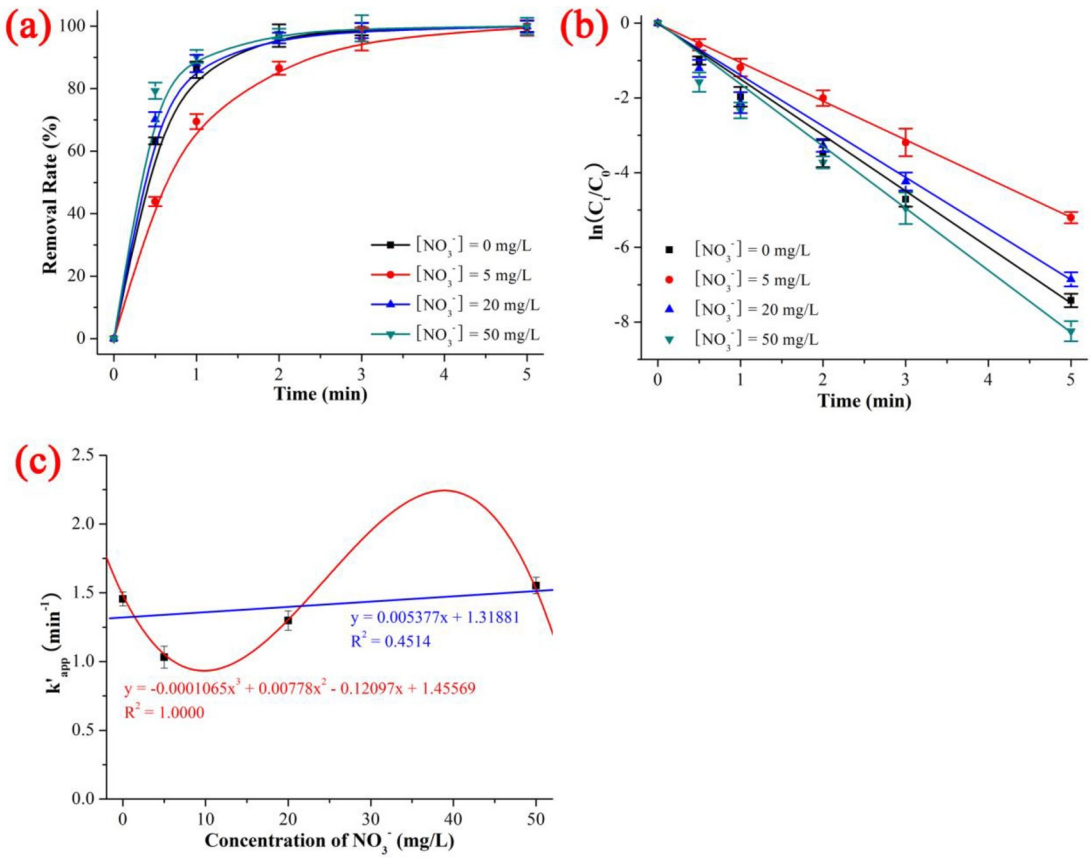

Fig 8. Effect of NO_3^- on the removal rate (a), kinetics constant (b) and linear fitting between kinetics constant and concentration of NO_3^- on the degradation of NIF *via* UV/H_2O_2. The error bars represent the standard deviation (n = 3).

https://doi.org/10.1371/journal.pone.0258483.g008

NO_3^- and ·OH is shown in (Eq 28) to (Eq 32) [40]:

$$NO_3^- + hv \rightarrow NO_2^- + O \quad \text{(Eq 28)}$$

$$NO_3^- + hv \rightarrow NO_2 \cdot + O\cdot^- \quad \text{(Eq 29)}$$

$$2\ NO_2 \cdot + H_2O \rightarrow NO_2^- + NO - + 2\ H^+ \quad \text{(Eq 30)}$$

$$O + H_2O \rightarrow 2 \cdot OH \quad \text{(Eq 31)}$$

$$O\cdot^- + H_2O \rightarrow \cdot OH + OH^- \quad \text{(Eq 32)}$$

In summary, the effect of co-existing anions was as follows: The divalent anions (SO_4^{2-} and CO_3^{2-}) caused a good linear decrease with increasing initial pH and concentration of divalent anions (R^2 of SO_4^{2-} and CO_3^{2-} was 0.9939 and 0.8589, respectively). The monovalent anions had a complex effect; Cl^- and NO_3^- had opposite effects on NIF degradation: low Cl^- and high NO_3^- promoted degradation, while high Cl^- and low NO_3^- inhibited degradation. The degradation kinetics of NIF *via* the UV/H_2O_2 system showed a poor linear decrease with increasing Cl^-/NO_3^- concentration (R^2 of Cl^- and NO_3^- was 0.5013 and 0.4514, respectively).

3.7 Oxidation mechanism and degradation pathway of NIF *via* UV/H_2O_2

In recent advances in UV/H_2O_2 systems, the degradation of organic pollutants has been due to the generation of ROS, especially ·OH and $\cdot O_2^-$. The oxidation mechanism of NIF degradation *via* the UV/H_2O_2 system was measured by ESR measurements, and the ESR spectra are shown in Fig 9A and 9B. The significant ·OH signal (Fig 9A) showed four peaks at 321.8 mT (P_A), 323.3 mT (P_B), 324.8 mT (P_C) and 326.3 mT (P_D). The interspaces of P_A-P_B, P_B-P_C and P_C-P_D were constant of 1.5 mT, and the intensity ratio of P_A, P_B, P_C and P_D was 1:2:2:1 [41]. The significant $\cdot O_2^-$ signal (Fig 9B) showed four peaks at 322.1 mT (P'_A), 323.2 mT (P'_B), 324.4 mT (P'_C) and 325.8 mT (P_D). The interspaces of P'_A-P'_B, P'_B-P'_C and P'_C-P'_D were constant within the range of 1.0 mT from 1.5 mT, and the intensity ratio of P'_A, P'_B, P'_C and P'_D was 1:1:1:1 [42]. However, the intensity of the ·OH signal was stronger than that of the $\cdot O_2^-$ signal, which means that ·OH was the primary key ROS and $\cdot O_2^-$ was the secondary key ROS. The oxidation mechanism of NIF degradation *via* the UV/H_2O_2 system is shown in (Eq 33) to (Eq 41) [43]. The generation of ·OH mainly comes from the direct decomposition of H_2O_2 (Eq 33), the generation of $\cdot O_2^-$ mainly comes from the indirect reaction between oxygen gas (dissolved oxygen and H_2O_2 decomposition) and electrons (Eqs 35 and 38), and NIF is degraded *via* the ROS (Eq 41) [44].

$$H_2O_2 + hv \rightarrow 2 \cdot OH \quad \text{(Eq 33)}$$

$$H_2O_2 + \cdot OH \rightarrow \cdot HO_2 + H_2O \quad \text{(Eq 34)}$$

$$\cdot HO_2 \rightarrow \cdot O_2^- + H^+ \quad \text{(Eq 35)}$$

$$2 \cdot HO_2 \rightarrow H_2O_2 + O_2 \quad \text{(Eq 36)}$$

$$\cdot HO_2 + \cdot OH \rightarrow H_2O + O_2 \quad \text{(Eq 37)}$$

$$O_2 + e^- \rightarrow \cdot O_2^- \quad \text{(Eq 38)}$$

$$2 \cdot O_2^- \rightarrow {}^1O_2 + {}^3O_2 + 2e^- \quad \text{(Eq 39)}$$

$$2 \cdot OH \rightarrow H_2O_2 \quad \text{(Eq 40)}$$

$$\text{NIF} + \text{ROS} \rightarrow \text{Intermediate Products} \rightarrow CO_2 + H_2O \quad \text{(Eq 41)}$$

The identification of intermediate NIF products *via* UV/H_2O_2 was performed using an Agilent 1260 series liquid chromatogram mass spectrometry (LC-Q-TOF-MS) system. The reaction conditions were: NIF concentration = 5 mg/L, pH = 7, H_2O_2 dose = 0.52 mmol/L, T = 20˚C and reaction time = 30 min. Preliminary analyses were conducted to evaluate the intermediate products of NIF produced by the UV/H_2O_2 method, and four kinds of NIF degradation intermediate products were observed in the mass spectrum based on the mass-to-charge (*m/z*) ratio. Four intermediate products were present: P345 (*m/z* = 345), P329 (*m/z* = 329), P315 (*m/z* = 315) and P274 (*m/z* = 274). The structures of P345, P329, P315 and P274 are shown in S3A–S3D Fig, respectively.

As shown in Fig 10A and 10B, the peak areas of all the observed products first increased and then decreased within 30 min. The peak areas of P345 and P274 at different reaction times

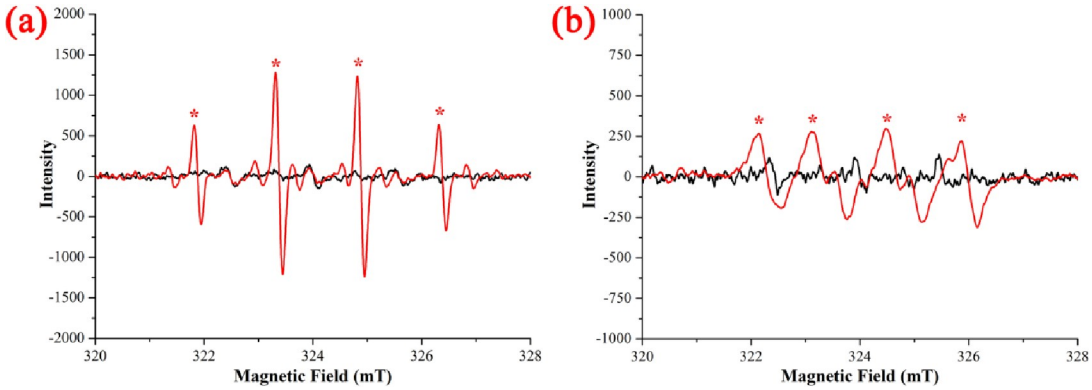

Fig 9. ESR measurements of ·OH (a) and ·O_2^- (b).

https://doi.org/10.1371/journal.pone.0258483.g009

are shown in Fig 10A, and the results indicated that the maximum peak area of P345 appeared at 5 min, the maximum peak area of P274 appeared at 20 min, and the peak intensity of P345 was stronger than that of P274. The first degradation pathway of NIF *via* the UV/H_2O_2 method was proposed as follows: protonated NIF ($C_{17}H_{19}N_2O_6^+$, *m/z* = 347) first lost H_2 to generate P345 ($C_{17}H_{17}N_2O_6^+$, *m/z* = 345) *via* dehydrogenation reaction, and then P345 lost C_3H_5NO to generate P274 ($C_{14}H_{12}NO_5^+$, *m/z* = 274), as shown in Fig 11A [45,46]. The peak areas of P329 and P315 at different reaction times are shown in Fig 10B, and the results indicated that the maximum peak area of P329 appeared at 0.5 min, the maximum peak area of P315 appeared at 7 min, and the peak intensity of P329 was stronger than that of P315. The second degradation pathway of NIF *via* the UV/H_2O_2 method was proposed as follows: protonated NIF ($C_{17}H_{19}N_2O_6^+$, *m/z* = 347) first lost H_2O to generate P329 ($C_{17}H_{17}N_2O_5^+$, *m/z* = 329) *via* dehydration reaction, and then P329 lost CH_2 to generate P315 ($C_{16}H_{15}N_2O_5^+$, *m/z* = 274), as shown in Fig 11B [45,46].

P315 was degraded with the attack of ROS. The intermediate products of P271 (*m/z* = 271), P241 (*m/z* = 241) and P181 (*m/z* = 181) are shown in S7 Table, and its possible degradation pathway is shown in S4A Fig. P315 first lost CO_2 to generate P271 ($C_{15}H_{15}N_2O_3^+$, *m/z* = 271), P271 lost CH_2O to generate P241 ($C_{14}H_{13}N_2O_2^+$, *m/z* = 241), and finally, P241 lost $C_2H_4O_2$ to generate P181 ($C_{12}H_9N_2^+$, *m/z* = 181) [46]. P329 was present as an isomeride that was named P329-2 (*m/z* = 329). The intermediate products, P329-2, P301 (*m/z* = 301), P200 (*m/z* = 200)

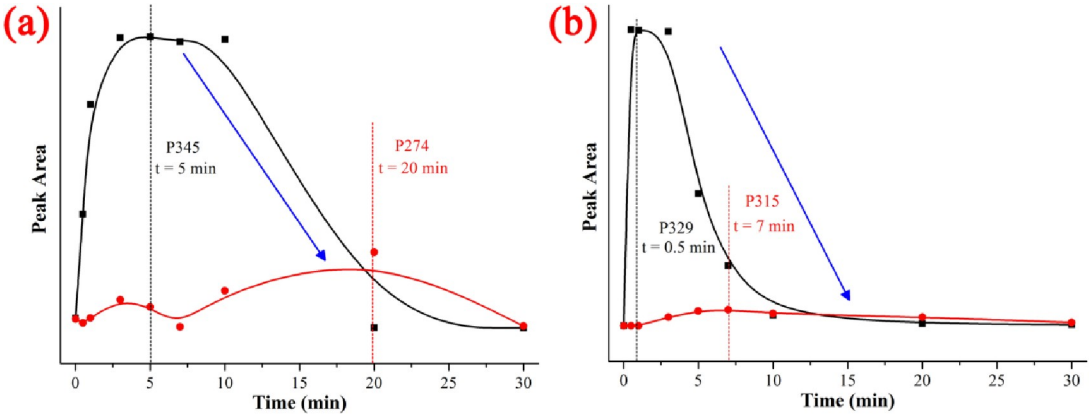

Fig 10. Chromatography of the intermediate products of NIF *via* UV/H_2O_2.

https://doi.org/10.1371/journal.pone.0258483.g010

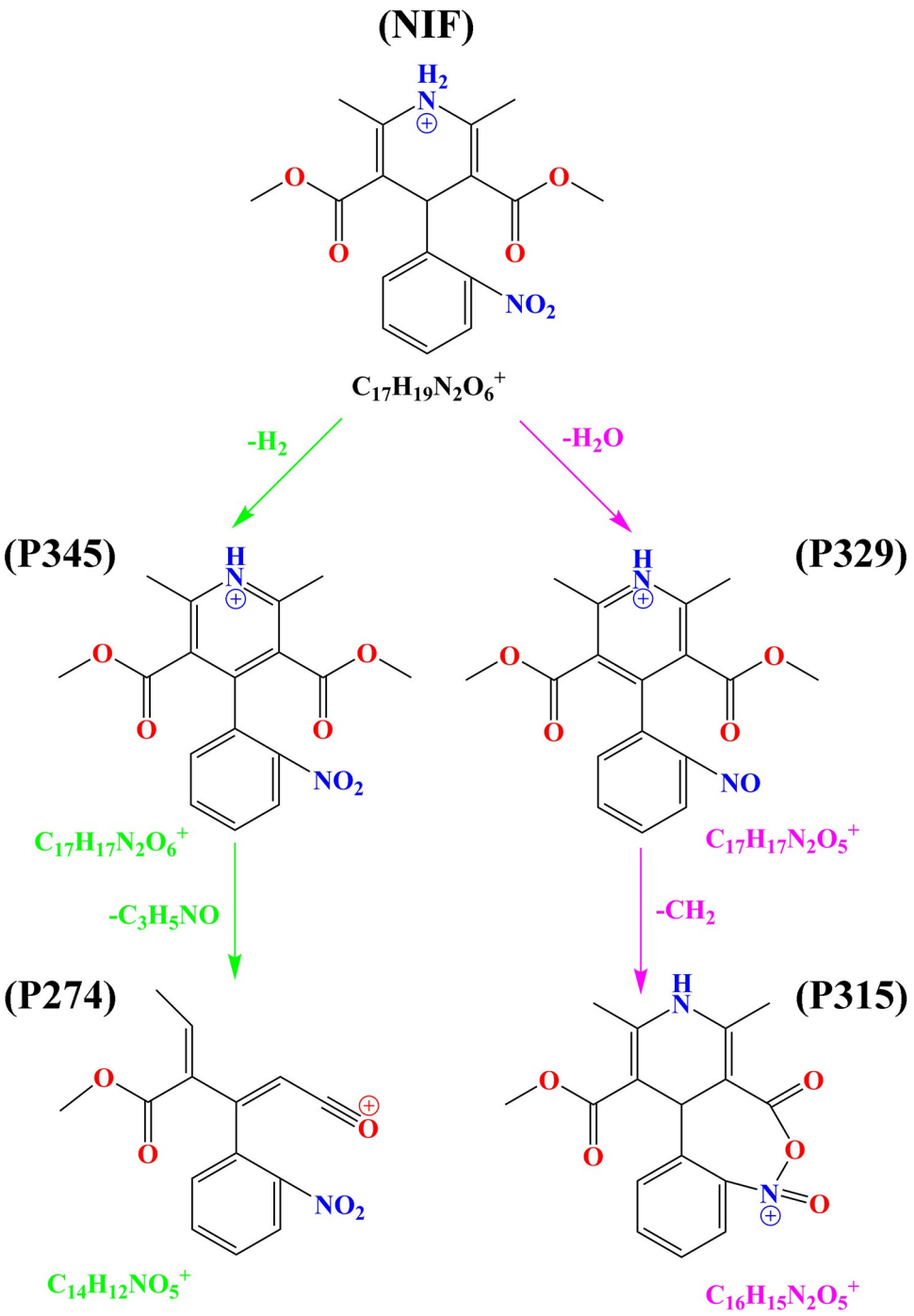

Fig 11. Degradation pathway of NIF *via* UV/H_2O_2 system.

https://doi.org/10.1371/journal.pone.0258483.g011

and P158 (m/z = 158), are shown in S7 Table, and their possible degradation pathways are shown in S4B Fig. P329-2 first lost CO to generate P301 ($C_{16}H_{17}N_2O_4^+$, m/z = 301), P301 lost $C_4H_7NO_2$ to generate P200 ($C_{12}H_{10}NO_2^+$, m/z = 200), and finally, P200 lost C_2H_2O to generate P158 ($C_{10}H_8NO^+$, m/z = 158) [46].

Table 1. Summary of removal performance of antibiotics *via* AOPs.

Technology	Pollutant	Removal Rate	k'_{app}	Time	Reference
UV/H_2O_2	NIF	99.94%	1.45569 min^{-1}	5 min	This work
Photo-degradation	NIF	65%	$(6.22\pm0.1)*10^{-5}$ s^{-1}	300 min	[29]
UV/H_2O_2	Norfloxacin	98.8%	0.22248 min^{-1}	20 min	[31]
Photocatalysis	Norfloxacin	97%		60 min	[49]
Photocatalysis	Norfloxacin	91%	0.02279 min^{-1}	90 min	[50]
Photocatalysis	Ciprofloxacin	92.3%	0.0438 min^{-1}	50 min	[51]
Photo-Fenton	Norfloxacin	90%	0.076 min^{-1}	120 min	[52]
O_3	Norfloxacin	>90%	0.1935 min^{-1}	15 min	[53]
MnO_x/SBA-15/O_3	Norfloxacin	>90%	0.3147 min^{-1}	15 min	[53]
Sonocatalysis	Norfloxacin	69.07%	0.0075 min^{-1}	150 min	[54]

https://doi.org/10.1371/journal.pone.0258483.t001

3.8 Environmental significance

In this paper, fast, effective and low-cost UV/H_2O_2 was used in the degradation of the antibiotic NIF, and this work contributed to the sustainable development of new methods for applications in hospital and aquaculture wastewater treatment for sustainable development, cleaner production and an environmentally friendly society, as shown in Table 1. The maximum degradation rate (99.94%), degradation kinetics constant (1.45569 min^{-1}) and minimum degradation time (5 min) indicated that the UV/H_2O_2 system is a promising AOP treatment for organic and medical wastewater. In addition, the cost of the UV/H_2O_2 system was approximately \$0.447 for 1 m^3 wastewater (S8 Table), which was lower than that of related systems (ranging from \$0.53 to \$0.85 for 1 m^3 wastewater) [47]. During the catalytic oxidation process, all the molecular mechanisms of ROS generation under the UV/H_2O_2 system, the effects of co-existing anions in an actual water environment, the analysis of intermediate products and the degradation pathways were the basis of the efficient AOP design. Furthermore, intermediate products and the degradation pathways of pollutants should also be studied through theoretical simulation technologies such as density functional theory (DFT) and molecular dynamics (MD) [48].

4 Conclusions

The degradation rate and degradation kinetics of NIF first increased and then remained constant as the H_2O_2 dose increased, and the quasi-percolation threshold was an H_2O_2 dose of 0.378 mmol/L. The effect of the initial pH, divalent anions (SO_4^{2-} and CO_3^{2-}) and monovalent anions (Cl^- and NO_3^-) decreased linearly with increasing initial pH and co-existing anions (the R^2 values of the initial pH, SO_4^{2-}, CO_3^{2-} Cl^- and NO_3^- were 0.6884, 0.9939, 0.8589, 0.5013 and 0.4514, respectively). ·OH was the primary key ROS, and $\cdot O_2^-$ was the secondary key ROS. There were 11 intermediate products (P345, P329, P329–2, P315, P301, P274, P271, P241, P200, P181 and P158) and 2 degradation pathways (dehydrogenation reaction of NIF → P345 → P274 and dehydration reaction of NIF → P329 → P315).

Supporting information

S1 Fig. UV-Vis absorption spectra of NIF.
(DOCX)

S2 Fig. Chromatography and standard curve of NIF.
(DOCX)

S3 Fig. Mass spectrum of intermediate products of NIF *via* UV/H_2O_2.
(DOCX)

S4 Fig. Possible degradation pathways of P315 and P329-2 in the UV/H_2O_2 system.
(DOCX)

S1 Table. Effect of H_2O_2 dose on the degradation of NIF *via* UV/H_2O_2. Reaction conditions: NIF concentration = 5 mg/L, H_2O_2 dose = 0–1.04 mmol/L, pH = 7, T = 20 ˚C and reaction time = 5 min.
(DOCX)

S2 Table. Effect of initial pH on the degradation of NIF via UV/H_2O_2.
(DOCX)

S3 Table. Effect of SO_4^{2-} on the degradation of NIF *via* UV/H_2O_2.
(DOCX)

S4 Table. Effect of CO_3^{2-} on the degradation of NIF *via* UV/H_2O_2.
(DOCX)

S5 Table. Effect of Cl^- on the degradation of NIF *via* UV/H_2O_2.
(DOCX)

S6 Table. Effect of NO_3^- on the degradation of NIF *via* UV/H_2O_2.
(DOCX)

S7 Table. Molecular weight, molecular formula, structural formula and *m/z* of intermediate products.
(DOCX)

S8 Table. Cost analysis of UV/H_2O_2 treatment.
(DOCX)

Author Contributions

Conceptualization: Wenping Dong, Chuanxi Yang, Lingli Zhang.

Data curation: Wenping Dong, Chuanxi Yang, Lingli Zhang.

Formal analysis: Chuanxi Yang, Lingli Zhang, Qiang Su, Xiaofeng Zou.

Funding acquisition: Weiliang Wang.

Investigation: Qiang Su.

Methodology: Qiang Su, Xiaofeng Zou, Kang Xie.

Software: Xiaofeng Zou.

Supervision: Weiliang Wang.

Validation: Wenfeng Xu, Xingang Gao, Kang Xie.

Visualization: Wenfeng Xu, Xingang Gao, Kang Xie.

Writing – original draft: Wenping Dong, Chuanxi Yang.

Writing – review & editing: Chuanxi Yang.

References

1. Li SL, Ren YH, Fu YY, Gao XS, Jiang C, Wu G, et al. Fate of artificial sweeteners through wastewater treatment plants and water treatment processes. Plos One. 2018; 13: e0189867. https://doi.org/10.1371/journal.pone.0189867 PMID: 29293534
2. Poulopoulos SG, Yerkinova A, Ulykbanova G, Inglezakis VJ. Photocatalytic treatment of organic pollutants in a synthetic wastewater using UV light and combinations of TiO_2, H_2O_2 and Fe(III). Plos One. 2019; 14: e0216745. https://doi.org/10.1371/journal.pone.0216745 PMID: 31091256
3. Liu YF, Ren J, Wang XR, Fan ZQ. Mechanism and reaction pathways for microcystin-LR degradation through UV/H_2O_2 treatment. Plos One. 2016; 11: e0156236. https://doi.org/10.1371/journal.pone.0156236 PMID: 27281173
4. Maafi W, Maafi M. Modelling nifedipine photodegradation, photostability and actinometric properties. Int J Pharmaceut. 2013; 456: 153–164.
5. Shim SC, Pae AN, Lee YJ. Mechanistic studies on the photodegradation of nifedipine. B Korean Chem Soc. 1988; 9: 271–274.
6. Onoue S, Igarashi N, Yamauchi Y, Murase N, Zhou Y, Kojima T, et al. In vitro phototoxicity of dihydropyridine derivatives: a photo-chemical and photobiological study. Eur J Pharm Sc. 2008; 33: 262–270.
7. Pizarro-Urzua NA, Nunez-Vergara LJ. Nifedipine and nitrodipine reactivity towards singlet oxygen. J Photoch Photobio A. 2005; 175: 129–137.
8. Chen JQ, Zheng FZ, Guo RX. Algal feedback and removal efficiency in a sequencing batch reactor algae process (SBAR) to treat the antibiotic cefradine. Plos One. 2015; 10: e0133273. https://doi.org/10.1371/journal.pone.0133273 PMID: 26177093
9. Garcia-Munoz P, Zussblatt NP, Pliego G, Zazo JA, Fresno F, Chmelka BF, et al. Evaluation of photoassisted treatments for norfloxacin removal in water using mesoporous Fe_2O_3-TiO_2 materials. J Environ Manage. 2019; 238: 243–250. https://doi.org/10.1016/j.jenvman.2019.02.109 PMID: 30852400
10. Luo JW, Li X, Ge CJ, Müller K, Yu HM, Huang P, et al. Sorption of norfloxacin, sulfamerazine and oxytetracycline by KOH-modified biochar under single and ternary systems. Bioresource Technol. 2018; 263: 385–392. https://doi.org/10.1016/j.biortech.2018.05.022 PMID: 29763802
11. Yang CX, Wang XN, Ji YJ, Ma T, Zhang F, Wang YQ, et al. Photocatalytic degradation of methylene blue with ZnO@C nanocomposites: Kinetics, mechanism, and the inhibition effect on monoamine oxidase A and B. NanoImpact. 2019; 15: 100174.
12. Chen MJ, Chu W. Photocatalytic degradation and decomposition mechanism of fluoroquinolones norfloxacin over bismuth tungstate: Experiment and mathematic model. Appl Catal B-Environ. 2015; 168–169: 175–182.
13. Hasija V, Raizada P, Singh P, Verma N, Khan AAP, Singh A, et al. Progress on the photocatalytic reduction of hexavalent Cr (VI) using engineered graphitic carbon nitride. Process Saf Environ. 2021; 152: 663–678.
14. Soni V, Raizada P, Singh P, Cuong HN, Rangabhashiyam S, Saini A, et al. Sustainable and green trends in using plant extracts for the synthesis of biogenic metal nanoparticles toward environmental and pharmaceutical advances: A review. Environ Res. 2021; 202: 111622. https://doi.org/10.1016/j.envres.2021.111622 PMID: 34245729
15. Gunarathne V, Rajapaksha AU, Vithanage M, Alessi DS, Selvasembian R, Naushad M, et al. Hydrometallurgical processes for heavy metals recovery from industrial sludges. Crit Rev Env Sci Tec. 2020; https://doi.org/10.1080/10643389.2020.1847949
16. Hariharan A, Harini V1, Sandhya S, Rangabhashiyam S. Waste *Musa acuminata* residue as a potential biosorbent for the removal of hexavalent chromium from synthetic wastewater. Biomass Convers Bior. 2020; https://doi.org/10.1007/s13399-020-01173-3
17. Rangabhashiyam S, Vijayaraghavan K, Jawad AH, Singh P, Singh P. Sustainable approach of batch and continuous biosorptive systems for praseodymium and thulium ions removal in mono and binary aqueous solutions. Environ Technol Inno. 2021; 23: 101581.
18. Selvasembian R, Gwenzi W, Chaukura N, Mthembu S. Recent advances in the polyurethane-based adsorbents for the decontamination of hazardous wastewater pollutants. J Hazard Mater. 2021; 417: 125960. https://doi.org/10.1016/j.jhazmat.2021.125960 PMID: 34229405
19. Kumar A, Raizada P, Hosseini-Bandegharaei A, Thakur VK, Nguyen VH, Singh P. C-, N-vacancies defect engineering polymeric carbon nitride meeting photocatalysis: Viewpoints and challenges. J Mater Chem A. 2020; 9: 111–153.
20. Raizada P, Sudhaik A, Singh P, Hosseini-Bandegharaei A, Thakur P. Converting type II AgBr/VO into ternary Z scheme photocatalyst via coupling with phosphorus doped g-C_3N_4 for enhanced photocatalytic activity. Sep Purif Technol. 2019; 227: 115692.

21. Hasija V, Sudhaik A, Raizada P, Hosseini-Bandegharaei A, Singh P. Carbon quantum dots supported AgI/ZnO/phosphorus doped graphitic carbon nitride as Z-scheme photocatalyst for efficient photodegradation of 2, 4-dinitrophenol. J Environ Chem Eng. 2019; 7: 103272.

22. Patial S, Raizada P, Hasija V, Singh P, Thakur VK, Nguyen VH. Recent advances in photocatalytic multivariate metal organic frameworks-based nanostructures toward renewable energy and the removal of environmental pollutants. Mater Today Energy. 2021; 19: 100589.

23. Kumar A, Raizada P, Singh P, Saini RV, Saini AK, Hosseini-Bandegharaei A. Perspective and status of polymeric graphitic carbon nitride based Z-scheme photocatalytic systems for sustainable photocatalytic water purifcation. Chem Eng J. 2020; 391: 123496.

24. Singh P, Shandilya P, Raizada P, Sudhaik A, Rahmani-Sani A, Hosseini-Bandegharaei A. Review on various strategies for enhancing photocatalytic activity of graphene based nanocomposites for water purification. Arab J Chem. 2020; 13: 3498–3520.

25. Raizada P, Kumari J, Shandilya P, Singh P. Kinetics of photocatalytic mineralization of oxytetracycline and ampicillin using activated carbon supported ZnO/ZnWO4 nanocomposite in simulated wastewater. Desalin Water Treat. 2017; 79: 204–213.

26. Raizada P, Sudhaik A, Singh P, Shandilya P, Gupta VK, Hosseini-Bandegharaei A, et al. Ag3PO4 modified phosphorus and sulphur co-doped graphitic carbon nitride as a direct Z-scheme photocatalyst for 2, 4-dimethyl phenol degradation. J Photoch Photobio A. 2019; 374: 22–35.

27. Sonu, Dutta V, Sharma S, Raizada P, Hosseini-Bandegharaei A, Gupta VK, Singh P. Review on augmentation in photocatalytic activity of CoFe2O4 via heterojunction formation for photocatalysis of organic pollutants in water. J Saudi Chem Soc. 2019; 23: 1119–1136.

28. Suzuki H, Fujiwara S, Kondo S, Sugimoto I. Determination of nifedipine in human plasma by high-performance liquid chromatography with electrochemical detection. J Chromatogr B. 1985; 341: 341–347. https://doi.org/10.1016/s0378-4347(00)84047-5 PMID: 4030984

29. Shamsipur M, Hemmateenejad B, Akhond M, Javidnia K, Miri R. A study of the photo-degradation kinetics of nifedipine by multivariate curve resolution analysis. J Pharmaceut Biomed. 2003; 31: 1013–1019. https://doi.org/10.1016/s0731-7085(02)00710-0 PMID: 12684114

30. Yao H, Sun PZ, Minakata D, Crittenden JC, Huang CH. Kinetics and modeling of degradation of ionophore antibiotics by UV and UV/H_2O_2. Environ Sci Technol. 2013; 47: 4581–4589. https://doi.org/10.1021/es3052685 PMID: 23570532

31. Yang CX, Wang XN, Zhang LL, Dong WP, Yang C, Shi XF, et al. Investigation of kinetics and mechanism for the degradation of antibiotic norfloxacin in wastewater by UV/H_2O_2. J Taiwan Inst Chem E. 2020; 115: 117–127.

32. Zhao Q, An JK, Wang S, Wang C, Liu J, Li N. Heterotopic formaldehyde biodegradation through UV/H_2O_2 system with biosynthetic H_2O_2. Water Environ Res. 2019; 91: 598–605. https://doi.org/10.1002/wer.1070 PMID: 30866122

33. Lu SY, Wang NY, Wang C. Oxidation and biotoxicity assessment of microcystin-LR using different AOPs based on UV, O_3 and H_2O_2. Front Env Sci Eng. 2018; 12: 12.

34. Kargar F, Barani Z, Salgado R, Debnath B, Lewis JS, Aytan Ee, et al. Thermal percolation threshold and thermal properties of composites with high loading of graphene and boron nitride fillers. ACS Appl Mater Inter. 2018; 10: 37555–37565. https://doi.org/10.1021/acsami.8b16616 PMID: 30299919

35. Santos LV, Meireles AM, Lange LC. Degradation of antibiotics norfloxacin by Fenton, UV and UV/H_2O_2. J Environ Manage. 2015; 154: 8–12. https://doi.org/10.1016/j.jenvman.2015.02.021 PMID: 25700351

36. Packer JL, Werner JJ, Latch DE, McNeill K, Arnold WA. Photochemical fate of pharmaceuticals in the environment: Naproxen, diclofenac, clofibric acid, and ibuprofen. Aquat Sci. 2003; 65: 342–351.

37. Hu LH, Flanders PM, Miller PL, Strathmann TJ. Oxidation of sulfamethoxazole and related antimicrobial agents by TiO_2 photocatalysis. Water Res. 2007; 41: 2612–2626. https://doi.org/10.1016/j.watres.2007.02.026 PMID: 17433403

38. Bhatkhande DS, Pangarkar VG, Beenackers AA. Photocatalytic degradation for environmental applications-a review. J Chem Technol Biot. 2001; 77: 102–116.

39. Liao CH, Kang SF, Wu FA. Hydroxyl radical scavenging role of chloride and bicarbonate ions in the UV/H_2O_2 process. Chemosphere. 2001; 44: 1193–1200. https://doi.org/10.1016/s0045-6535(00)00278-2 PMID: 11513408

40. Lu MC, Chen JN, Chang CP. Effect of inorganic ions on the oxidation of dichlorvos insecticide with Fenton's reagent. Chemosphere. 1997; 35: 2285–2293.

41. Yang CX, Dong WP, Cui GW, Zhao YQ, Shi XF, Xia XY, et al. Highly-efficient photocatalytic degradation of methylene blue by PoPD-modified TiO_2 nanocomposites due to photosensitization-synergetic effect of TiO_2 with PoPD. Scie Rep-UK. 2017; 7: 3973. https://doi.org/10.1038/s41598-017-04398-x PMID: 28638067

42. Lin YM, Li DZ, Hu JH, Xiao GC, Wang JX, Li WJ, et al. Highly efficient photocatalytic degradation of organic pollutants by PANI-modified TiO_2 composite. J Phys Chem C. 2012; 116: 5764–5772.

43. Yang CX, Dong WP, Cui GW, Zhao YQ, Shi XF, Xia XY, et al. Enhanced photocatalytic activity of PANI/TiO_2 due to their photosensitization-synergetic effect. Electrochim Acta. 2017; 247: 486–495.

44. Yang CX, Zhang M, Dong WP, Cui GW, Ren ZM, Wang WL. Highly efficient photocatalytic degradation of methylene blue by PoPD/TiO_2 nanocomposite. Plos One. 2017; 12: e0174104. https://doi.org/10.1371/journal.pone.0174104 PMID: 28329007

45. Pietta P, Rava A, Biondi P. High-performance liquid chromatography of nifefipine, its metabolites and photochemical degradation products. J Chromatogr A. 1981; 210: 516–521. https://doi.org/10.1016/s0021-9673(00)80344-1 PMID: 7251729

46. Handa T, Singh S, Singh IP. Characterization of a new degradation product of nifedipine formed on catalysis by atenolol: A typical case of alteration of degradation pathway of one drug by another. J Pharmaceut Biomed. 2014; 89: 6–17.

47. Steven R. Municipal water supply and sewage treatment: Costs, prices, and distortions. Canadian Journal of Economics/Revue canadienne d'économique. 1999; 32: 688–704.

48. Armaković S, Armaković SJ, Abramović BF. Theoretical investigation of loratadine reactivity in order to understand its degradation properties: DFT and MD study. J Mol Model. 2016; 22: 1–14. https://doi.org/10.1007/s00894-015-2876-x PMID: 26645805

49. Sturini M, Speltini A, Maraschi F, Pretali L, Ferri EN, Profumo A. Sunlight-induced degradation of fluoroquinolones in wastewater effluent: Photoproducts identification and toxicity. Chemosphere. 2015; 134: 313–318. https://doi.org/10.1016/j.chemosphere.2015.04.081 PMID: 25966937

50. Yin F, Wang C, Lin KYA, Tong SP. Persulfate activation for efficient degradation of norfloxacin by a rGO-Fe_3O_4 composite. J Taiwan Inst Chem E. 2019; 102: 163–169.

51. Wang FL, Feng YP, Chen P, Wang YF, Su YH, Zhang, et al. Photocatalytic degradation of fluoroquinolone antibiotics using ordered mesoporous g-C3N4 under simulated sunlight irradiation: Kinetics, mechanism, and antibacterial activity elimination. Appl Catal B-Environ. 2018; 227: 114–122.

52. Wammer KH, Korte AR, Lundeen RA, Sundberg JE, McNeill K, Arnold WA. Direct photochemistry of three fluoroquinolone antibacterials: Norfloxacin, ofloxacin, and enrofloxacin. Water Res. 2013; 47: 439–448. https://doi.org/10.1016/j.watres.2012.10.025 PMID: 23141476

53. Li J, Ji QQ, Lai B, Yuan DH. Degradation of p-nitrophenol by Fe^0/H_2O_2/persulfate system: Optimization, performance and mechanisms. J Taiwan Inst Chem E. 2017; 80: 686–694.

54. Juang RS, Chen CH. Comparative study on photocatalytic degradation of methomyl and parathion over UV-irradiated TiO_2 particles in aqueous solutions. J Taiwan Inst Chem E. 2014; 45: 989–995.